Engineering IL-2R agonists responsive to lactate-rich tumor microenvironments

Xudong Tang, Qiwen Jiang, Ziyan Yu, Meng Sun, Xuantong Liu, Yang Jin, Xinxin Zhang, Binxuan Zhang, Fan Yang, Kaiqing Zhang, Yinran Luo, Meng Guo*, Jianhua Luo*

*Correspondence to: Meng Guo (guom@immunol.org), Jianhua Luo (luojh@immunol.org)

Abstract

Adoptive cell therapy (ACT) for solid tumors, particularly pancreatic cancer, is limited by the immunosuppressive tumor microenvironment (TME), where low pH accelerates cytokine degradation and hinders receptor oligomerization. The efficacy of cellular therapeutics is further reduced by the IL-2 receptor (IL-2R) expression profile, as low-dose IL-2 preferentially activates regulatory T cells (T_{reg}), whereas high-dose administration induces systemic toxicity and vascular leak syndrome. Here, we applied *de novo* design to generate an acid-responsive IL-2R agonist that selectively engages IL-2Rβγ while sparing IL-2Rα. Using RFdiffusion, we created 100 IL-2Rβγ agonists and identified high-affinity candidates through AlphaFold3 and HDOCK screening. To confer pH sensitivity, we incorporated the GALA peptide, which folds into an amphipathic α-helix at low pH to promote receptor oligomerization. The optimized agonist, B51G35R-G, exhibited high-affinity binding to IL-2Rβγ but weak IL-2Rα interaction, enabling cytokine-independent activation, enhanced degranulation and improved tumor cytotoxicity of effector cells.

Keywords: IL-2 mimic, adoptive cell therapy, solid tumor, receptor oligomerization, pH-responsive

Introduction

Adoptive cell therapy (ACT) has revolutionized clinical treatment strategy, however, it continues to face considerable challenges when treating solid tumors (*1*). These limitations largely arise from immunosuppressive tumor microenvironment (TME), which is characterized by acidity, physical barriers and over-expressed checkpoints (*2, 3*). Meanwhile, cytokines essential for proliferation, activation and survival of immune cell, particularly interleukin-2 (IL-2) remain scarce (*4*). Besides, its therapeutic potential is significantly compromised within the acidic TME, where reduced stability accelerates IL-2 degradation (*5*). Collectively, these mechanisms culminate in exhaustion and impaired activation of effector cells.

The interleukin-2 receptor (IL-2R) is a heterotrimeric complex composed of three subunits: the α chain (CD25), which confers high-affinity binding of IL-2; the β chain (CD122) and γ chain (CD132), which mediates JAK-STAT signaling through receptor oligomerization, a process frequently impaired under acidic conditions that limits IL-2 activity within the TME (*6, 7*). Therapeutically, IL-2 embodies a paradox, as low doses preferentially expand T_{reg} through their high IL-2Rα expression and promote immunosuppression (*8*), whereas high doses activate vascular endothelium and increase permeability, resulting in systemic toxicity and vascular leak syndrome (*9*).

De novo protein design enables the rational construction of novel protein sequences endowed with predetermined structural and functional properties (*10, 11*). In this project, we generated two distinct libraries of 100 candidates each targeting IL-2Rβ and IL-2Rγ via RFdiffusion. After HDOCK screening to eliminate sequences with high IL-2Rα affinity, we randomly assembled selected β and γ agonists and subjected them to structural prediction with AlphaFold3 (AF3) followed by experimental validation. From these, three combinations-B34G35R, B51G35R, and B51G9-were identified, all exhibiting low affinity for IL-2Rα but high-affinity binding to IL-2Rβγ. To confer pH sensitivity, we incorporated the GALA peptide, which contracts into an amphipathic α-helix under acidic conditions but remains extended at neutral pH, as a linker to promote IL-2R oligomerization. Among these, GALA modified B51G35R (B51G35R-G)

demonstrated the strongest IL-2Rβγ binding and enabled IL-2R oligomerization exclusively under acidic conditions. Effector cells engineered with B51G35R-G displayed robust proliferation, enhanced activation, and markedly improved anti-tumor efficacy. Collectively, our strategy leverages the rational *de novo* design of an acid-responsive IL-2 receptor agonist that circumvents T_{reg} activation and selectively empowers effector cells within the hostile tumor microenvironment.

Results

Developing peptide for selectively binding of IL-2Rβ and IL-2Rγ via *de novo* design

Based on the natural binding sites between IL-2 and IL-2Rβ and γ (Fig. 1a), we employed RFdiffusion to perform *de novo* design, generating 100 mimics with high affinity for IL-2Rβ or γ but low affinity for IL-2Rα respectively, each with a length ranging from 46-65 amino acids (Fig. 1b and Extended Data Table 1 and 2). Selection was based on the principle that lower docking scores indicate higher binding affinity. To avoid high affinity for IL-2Rα, sequences exhibiting docking scores below -218 with IL-2Rβ, yet above -215 with IL-2Rα, including B0, B34, and B51 were selected (Extended Data Table 3). Meanwhile, sequences with scores lower than -240 against IL-2Rγ but higher than -245 against IL-2Rα, namely G9, G16, G26, G32, G35, G42, G57, G63, G71, G88, and G90, were included (Extended Data Table 4).

Through visual inspection with PyMOL to obtain the tightly packed helical bundles with a high likelihood of expression as recombinant proteins, we ultimately selected B0, B34, and B51, along with G9, G16, G35, G42, G57, and G71 based on their binding interface to the IL-2R (Fig. 1c). However, the results indicated that most amino acids primarily contributed to structural stability rather than mediating IL-2R binding. Therefore, candidate sequences were truncated to 20 residues directly involved in binding interface contacts, whereas B34 was retained as a 39-amino acid construct to preserve its dispersed interaction sites (Fig. 1d and Extended Data Table 5 and 6).

Screening and affinity evaluation of IL-2Rβγ agonists

G9, G16, G35, G42, G57, and G71, together with their reverse counterparts, were conjugated via a flexible linker and fused with a glycosylphosphatidylinositol (GPI) anchor to retain IL-2 mimics on the cell surface, while incorporation of a Flag tag enabled subsequent detection and isolation, collectively facilitating NK cell activation (Fig. 2a) Lentiviral transduction of NK-92 cells generated a library of 36 variants, each expressing a distinct IL-2 mimic. To identify the specific sequences that promote NK cell proliferation, the library was seeded into 96-well plates at one cell per well and cultured under cytokine-free conditions. Expanded clones were subsequently harvested and subjected to sequencing (Fig. 2a), which revealed significant enrichment of B34G35R, B51G35R, and B51G9 compared with other constructs (Fig. 2b).

To define the protein-protein interfaces for residue-wise flexibility (B-factor), electrostatic, and van der Waals interaction energy fluctuations, molecular dynamics (MD) simulations were employed to evaluate the affinity of designed IL-2 mimics towards the IL-2Rβγ subunits. Higher RMSD values in the B34G35R complex indicated an unstable receptor binding mode, in contrast to the lower RMSD and enhanced stability observed in the B51G35R complexes (Fig. 2c). The radar plot based on flexibility and conformational entropy features revealed that B51G9 exhibited the lowest conformational diversity and minimal interaction energy fluctuations at the binding interface, suggesting high structural consistency and binding stability, yet a higher B-factor suggested greater atomic uncertainty (Fig. 2d). By contrast, B51G35R showed consistently lower values across all three dimensions, suggesting superior structural stability and identifying it as one of the most promising complexes (Fig. 2d). Bio-layer interferometry (BLI) characterization of binding to IL-2Rα and IL-2Rβγ immobilized on Octet sensor chips revealed KD values separately. In the screening for mimics with low IL-2Rα but high IL-2Rβγ affinity, B51G35R demonstrated the weakest binding to IL-2Rα, substantially below IL-2 (Fig. 2e), while demonstrating the highest affinity toward IL-2Rβ and IL-2Rγ among all tested variants (Fig. 2f). Collectively, these findings establish B51G35R as a selective IL-2Rβγ agonist that minimizes IL-2Rα interaction while preserving high-affinity binding to IL-2Rβγ.

Selective IL-2Rβγ agonists modulate functions of effector cells

After confirming their binding affinity to IL-2R, we systematically evaluated B34G35R, B51G35R, and B51G9 for their capacity to enhance NK cell proliferation, activation, and cytotoxicity, thereby identifying the most effective IL-2 mimics. Among these, B51G35R demonstrated superior potency in driving NK cell expansion compared with native IL-2 (Fig. 3a), and its advantage was further validated in YT cells (Fig. 3b). We further armed αMSLN CAR-NK and αHER2 CAR-T cells with the IL-2 mimics and measured their tumor-killing activity. The heatmap showed that cells expressing B51G35R achieved optimal killing efficacy, outperforming the other two constructs. In contrast, B51G9 only marginally enhanced cytotoxic activity (Fig. 3c).

Effector cell activation and effector molecule secretion were concurrently evaluated. NK cells stimulated with B51G35R displayed markedly enhanced activity, as indicated by increased expression of the degranulation marker CD107a and the activation marker CD69 (Fig. 3d-e). Both B51G9 and B51G35R stimulation significantly increased perforin (PFN) production compared with IL-2. Notably, B51G9 induced substantially higher granzyme B (GrB) secretion than B51G35R, suggesting distinct functional profiles between the mimics (Fig. 3f).

Design and affinity characterization of acid-responsive IL-2 Mimics

To address the limitation that IL-2 fails to promote receptor oligomerization under acidic conditions, the linker in B34G35R, B51G35R, and B51G9 were substituted with GALA4, GALA5, or GALA6 (Fig. 4a). The GALA peptide is a synthetically designed, pH-sensitive motif that transitions from a random coil to an amphipathic α-helix as the pH decreases from 7.0 to 5.0, a property anticipated to drive receptor oligomerization specifically in acidic environments (Fig. 4b). Using AF3, we first assessed the binding interfaces between IL-2Rβγ and the GALA-modified mimics. The results demonstrated that incorporation of the GALA peptide neither compromised structural positioning nor interfered with receptor-binding interactions. Guided by AF3 predicted TM-score (ptm) and inter-residue predicted TM-score (iptm), the GALA5 variant was selected for further experimental validation (Extended Data Table 7). The resulting constructs

incorporating GALA5 as a linker are hereafter referred to as B34G35R-G, B51G35R-G, and B51G9-G (Fig. 4c). Subsequent BLI assays under acidic conditions (pH 6.4, acidified with 15 mM lactate) revealed that all three mimics exhibited higher IL-2Rβγ affinity than IL-2, with B34G35R-G (52 pM) displaying substantially stronger binding than the other variants, indicating that GALA-modified IL-2 mimics possess acid-responsive binding capability (Fig. 4d).

Impact of acid-responsive IL-2R agonists on effector cell receptor oligomerization and functional potency

We evaluated the efficiency of IL-2Rβ/γ oligomerization induced by GALA-linked IL-2 mimics under acidic conditions using the NanoBiT protein complementation assay where the LargeBit and SmallBit fragments were fused to IL-2Rβ and IL-2Rγ, respectively (Fig. 5a). Upon stimulation with the IL-2, B34G35R-G, B51G35R-G and B51G9-G respectively, NanoBiT complementation signals revealed pronounced co-clustering of IL-2Rβ and IL-2Rγ at the plasma membrane compared with IL-2 stimulation alone, visualized as distinct fluorescent puncta. These findings demonstrate that B34G35R-G, B51G35R-G, and B51G9-G, effectively promote IL-2R oligomerization under acidic conditions (pH=6.4) (Fig. 5b).

We evaluated the ability of B34G35R-G, B51G35R-G, and B51G9-G to activate effector cells under different pH conditions. At physiological pH (7.4), B34G35R, B51G35R, and B51G9 strongly induced STAT5 phosphorylation, whereas B51G9-G triggered only mild IL-2R signaling in NK-92 cells, and neither B34G35R-G nor B51G35R-G elevated STAT5 phosphorylation (Fig. 5c, left). In contrast, under acidic conditions (pH 6.4), B34G35R-G and B51G35R-G induced robust STAT5 phosphorylation in NK cells, whereas unmodified constructs completely lost activity (Fig. 5c, right).

Assessment of NK cell expansion revealed that at physiological pH (7.4), the engineered variants B34G35R-G, B51G35R-G, and B51G9-G failed to enhance the tumor-killing efficacy of NK-92 cells. Notably, their activity was exclusively triggered under acidic conditions (pH 6.4). Among them, B51G35R-G exhibited the most potent

proliferative capacity, markedly surpassing B34G35R-G and B51G9-G. In sharp contrast, the proliferative activity driven by the non-GALA-modified variants and IL-2 was abolished at pH 6.4 (Fig. 5d). We next evaluated the anti-tumor activity of αMSLN CAR-NK cells expressing these acid-responsive IL-2R agonists. Critically, only under an acidic environment did B34G35R-G and B51G35R-G substantially enhance NK cell cytotoxicity, significantly exceeding their non-GALA-modified counterparts (Fig. 5e). Consistently, changes in CD107a expression as well as PFN and GrB production mirrored these trends (Fig. 5f-h). Collectively, these findings demonstrate that B34G35R-G, B51G35R-G, and B51G9-G are acid-responsive IL-2R agonists capable of significantly enhancing effector cell cytotoxicity under acidic conditions.

Discussion

This study utilized a *de novo* protein design approach to develop an innovative IL-2 mimic capable of selectively binding IL-2Rβ/γ with high affinity excluding interaction with IL-2Rα. This selective targeting decouples the dual immunomodulatory effects that IL-2 exerts on effector T cells and T_{reg} cells. Traditional protein engineering has enabled the rational construction of libraries through targeted mutations at key residues. Nevertheless, its application remains challenging for proteins with complex multi-subunit architectures (*12*). Unlike traditional approaches, *de novo* design begins with random noise and iteratively refines structures through a diffusion process, enabling the generation of highly distinctive mimics that transcend natural structural constraints. In this work, we performed *de novo* design of IL-2 mimics, specifically targeting the IL-2Rβγ subunits via RFdiffusion. This strategy leverages computational power to guide IL-2 evolution, thereby accelerating directed evolution (*13*).

The IL-2Rα is critical for initiating IL-2 receptor complex assembly yet does not participate in downstream signal transduction, despite its high affinity for IL-2. Resting T cells and NK cells constitutively lack IL-2Rα, acquiring IL-2 sensitivity only upon T-cell activation (*14*). However, its high expression on T_{reg} enables their activation by

low-dose IL-2, subsequently suppressing anti-tumor activity (*15*) (*16*). Our *de novo* design strategy bypasses natural templates, thereby directly preventing interaction with IL-2Rα (*12, 17-19*). *In vitro* validation confirmed that our mimics successfully abolished IL-2Rα binding while maintaining high affinity for IL-2Rβγ, effectively avoiding T_{reg} activation.

To further enhance the therapeutic potential of IL-2 mimics in solid tumors, we incorporated an acid-responsive design module by arming the mimics with the GALA peptide. Acidity is a hallmark physical feature of the TME in solid tumors, which can compromise ACT efficacy through altering the charge properties, thereby disrupting their structural integrity and transmembrane efficiency and directly suppressing the infiltration (*20*) and tumor-killing capacity (*21*). Given the prevalence of this acidic TME in solid tumors, targeting the TME itself presents a broader therapeutic avenue than targeting specific tumor antigens, especially for combating high tumor heterogeneity (*22*). Current ACT strategies focusing on the acidic TME primarily fall into two categories: passive acid-responsive approaches (*23-26*) and active correction of the acidic environment (*27, 28*). To confer pH sensitivity, we incorporated the GALA peptide, which adopts an amphipathic α-helical structure under acidic conditions but remains extended at neutral pH, as a linker to promote IL-2R oligomerization. This strategy enabled selective IL-2Rβγ dimerization of effector cells exclusively under acidic conditions, thereby mitigating the adverse effects associated with high-dose IL-2 while more effectively activating effector cells. This acid-responsive engineering provides a novel strategy for targeting the acidic microenvironment of solid tumors. Through the *de novo* design of an acid-responsive IL-2 mimic, this study demonstrates its strategies in protein engineering, particularly for complex cytokines that interact with multi-subunit receptors.

Methods

Cell lines

NK-92 and YT was obtained from the Immocell company (Immocell Biotechnology Co., Ltd., Xiamen, China). αMSLN CAR-NK were generated by lentiviral transduction. Cell lines were cultured in DMEM medium (Gibco), containing 10% fetal bovine serum (FBS). All cell lines were tested negative for mycoplasma.

De novo design using RFdiffusion, ProteinMPNN and AF3

RFdiffusion model weights and code were obtained from the RFdiffusion GitHub repository (https://github.com/RosettaCommons/RFdiffusion). The crystal structure of IL-2R (PDB ID: 2B5I) was used as the input template. A total of 5,500 diffused designs were generated using RFdiffusion, with all peptide residues defined as hotspots to maximize binding driven by the peptide rather than native IL-2R. For each backbone structure, four amino acid sequences of IL-2Rβγ binders were generated using ProteinMPNN and initially scored with AlphaFold3 (AF3). ProteinMPNN weights and code were obtained from the dl_binder_design GitHub repository (https://github.com/nrbennet/dl_binder_design), and AF3 predictions were run via the online server (https://deepmind.google/technologies/alphafold/alphafold-server/). Candidate binders were filtered based on the predicted interaction alignment error (ipAE) of the IL-2Rβγ–binder complex and the predicted local distance difference test (pLDDT). Designs with an ipAE below 12 Å and a pLDDT above 88 were selected for further optimization. Selected candidates were further filtered for unique RFdiffusion backbones to maximize structural diversity. Following this initial selection, the binders were subjected to sequence diversification. At the default sampling temperature (t = 0.1), 100 sequences were generated per initial binder design and re-evaluated by AF3, after which ipAE and pLDDT metrics were extracted as described above.

Lentivirus Preparation and Cell Construction

Lentivirus were generated using Lenti-X 293T cell line and packaging plasmid vectors. Twenty-four hours before transfection, 2×10^7 Lenti-X 293T cells were seeded in a 150-

mm culture dish. Next, lentivirus were transfected into packaging cells with psPAX2 and pMD2.G envelop plasmids, at a ratio of 4:3:1, using calcium-phosphate kit (ViralTherapy, R001) in accordance with the manufacturer's protocol. Supernatants were harvested after 48 and 72 h post-transfection and then they were concentrated by ultracentrifugation for 2.5 hours at 82,700 g at 4°C. Precipitated lentiviral particles were resuspended in Opti-MEM medium (Solarbio, 31985070). Lentiviral titer was determined using QuickTiter Lentivirus Quantitation Kit (Cell Biolabs, VPK-107) following the manufacturer's instructions.

Infection of NK-92 cell line

Collect NK-92 cells from a culture flask. Centrifuge at 300 × g for 5 minutes at room temperature. After careful removal of the supernatant, the cell pellet is resuspended in an appropriate volume of complete medium. Calculate the required volume of cell suspension to achieve a final concentration of 1×10^7 cells/mL. Add the calculated volume of cells to an appropriate volume of complete medium to achieve a final concentration of 1×10^7 cells/mL. Dispense 100 μL of the 1×10^7 cells/mL suspension into each well of a 96-well plate. Incubate the plates at 37°C in a 5% CO_2 incubator for 24 hours to achieve approximately 50% confluence using a light microscope to observe the cells. At 50% confluence, the cells should cover approximately half of the well surface. Some areas showed dense cell layers while others with less or no cells. To each well, 4μL of a 25 × polybrene infection-enhancing solution was added. Considering the multiplicity of infection (MOI) and the virus titer, the specific volume of the virus, calculated as (MOI × cell number) /virus titer, was added to the wells. The plates were then incubated at 37°C for 12-16 hrs.

Bio-layer interferometry

The binding data were collected in an Octet RED96 (Fortebio) and processed using the instrument's integrated software. To measure the affinity of peptide binders, N-terminally biotinylated target peptides with a short linker (GGS) were loaded onto streptavidin-coated biosensors (SA ForteBio) at 10nM in binding buffer (PBTS buffer (0.02% Tween 20, pH 7.4), MES Assay buffer (20 mM 2-Morpholinoethanesulfonic acid sodium salt, 200 mM NaCl, 0.1% BSA, 0.1% Tween-20, pH 6.0) for 120 s. Analyte

proteins were diluted from concentrated stocks into the binding buffer. After baseline measurement in the binding buffer alone, the binding kinetics were monitored by dipping the biosensors in wells containing the target protein at the indicated concentration and then dipping the sensors back into baseline buffer (dissociation).

Measurement of lactate dehydrogenase (LDH) activity

At the end of the incubation period, cytotoxicity was evaluated by measuring lactate dehydrogenase (LDH) activity (CytoTox 96® Non-Radioactive Cytotoxicity Assay kit; Promega G1780) according to manufacturers' instructions. Briefly, 100 μL cell-culture medium from each well from the 96-well plate was collected and transferred to the wells at E: T ratios of 1:1, and control groups were set. The 96-well plate was incubated at 37 °C with 5% CO_2 for 4 hours, and centrifuged at 250 g for 3 minutes. Afterwards 50 μL of supernatant was transferred from each well to a corresponding flat-bottom plate. The reconstituted substrate mix (50 μL) was added to all wells and let stand, protected from light at room temperature (25 °C) for 30 min. 50 μL of the Stop solution was added to each well and the plate was taken to read the absorbance at 490 nm and 680nm in a microplate spectrophotometer reader. Background signals (cell culture medium) were subtracted from the sample readings at 680 nm (background signal) from the absorbance at 490 nm (D). An LDH positive control supplied with the kit was used to validate the assay. Percentages (%) of NK cell killing and lysis (%) (percentage of LDH release) were determined using the formula: Lysis (%) = $[LDH^{E:T} - LDH^{E}]/LDH^{Max} \times 100\%$.

Flow cytometry

The effector cells were collected after 4 hrs of co-culture with tumor cells. Then, they were centrifuged 1×10^5 to 1×10^7 at 4 °C for 5 mins at 250 g and the supernatant was discarded. The cells are resuspended in 100 μL of FACS buffer. Preparation of experimental groups: experimental groups, a blank control group, an isotype control group, and a single stain control group were set up. The blocking of Fc receptors on cell surface: 0.5 μL of Fc receptor antibody was added and the mixture was incubated in the dark at 4 °C for 30 mins. The binding of fluorescent antibodies to cells: 1 μL of

fluorescent antibody was added and the mixture was incubated in the dark at 4 °C for 30 mins. Pre-cooled PBS was added to remove unbound fluorescent antibodies. Then the cells were centrifuged at 1500 g for 5 mins and the supernatant was discarded. This step was repeated twice. The cells were resuspended in 500 μL of PBS solution before loading. Flow cytometry analysis was performed.

NanoBit assay

In the NanoBiT-based assay designed to detect the interaction between IL-2Rβ and IL-2Rγ, the LargeBiT (LgBiT) subunit was fused to the C-terminus of IL-2Rβ (LgBiT-IL-2Rβ), while the SmallBiT (SmBiT) peptide was fused to the C-terminus of IL-2Rγ (SmBiT-IL-2Rγ). Suspension-adapted NK-92 cells were maintained in NK-92 specific serum-free medium supplemented with 500 IU/mL recombinant human IL-2 or IL-2 mimic. For transfection, cells were transfected using ViaFect™ Transfection Reagent (optimized for suspension cells) with a total of 800 ng plasmid mixture, consisting of 100 ng SmBiT-IL-2Rγ, 500 ng LgBiT-IL-2Rβ, and 200 ng empty vector as carrier DNA. After 24 hours of incubation, cells were harvested by centrifugation, resuspended in an appropriate assay buffer, and plated onto poly-L-lysine-coated glass-bottom dishes to facilitate adhesion during staining. Cells were then treated with either the IL-2 mimic or control buffer for 15 minutes at room temperature, fixed with 4% paraformaldehyde, and stained with primary antibodies against IL-2Rβ and IL-2Rγ, followed by fluorescently labeled secondary antibodies. These images were spectrally unmixed using single stain positive control images in the InForm software (Akoya Biosciences, Marlborough, Massachusetts, USA).

Western-blot

Cells were lysed with cold lysis buffer (Cell Signaling Technology, Danvers, Massachusetts, U.S.) supplemented with protease inhibitor mixture (Calbiochem, Darmstadt, Germany). The total protein concentration was measured using the BCA assay (Pierce, Rockford, IL) and was equalized with the extraction reagent. Protein extracts were separated by 10% SDS-PAGE, followed by electrophoretic transfer onto nitrocellulose membranes for Western blot analysis.

Statistical analysis

Unless otherwise specified, Student's t-test was used to evaluate the significance of differences between 2 groups, and analysis of variance (ANOVA) was used to evaluate differences among 3 or more groups. Survival analysis was performed by Kaplan-Meier survival analysis. Differences between samples were considered significant when $P<0.05$.

Figures

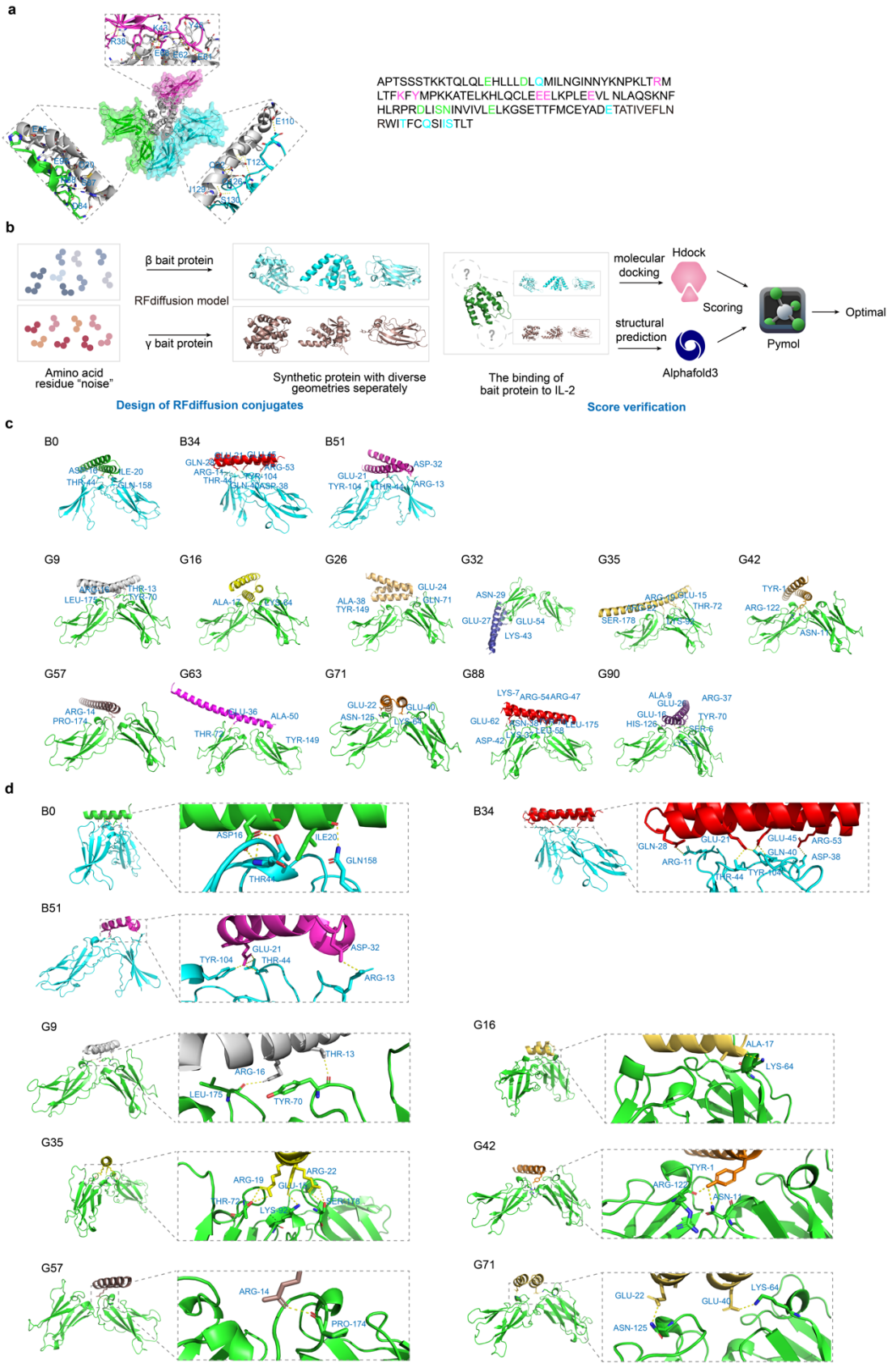
a
APTSSSTKKTQLQLEHLLLDLQMILNGINNYKNPKLTRM
LTFKFYMPKKATELKHLQCLEEELKPLEEVL NLAQSKNF
HLRPRDLISNINVIVLELKGSETTFMCEYADETATIVEFLN
RWITFCQSIISTLT
b
β bait protein
RFdiffusion model
γ bait protein
Amino acid residue "noise"
Synthetic protein with diverse geometries seperately
Design of RFdiffusion conjugates
molecular docking
Hdock
Scoring
structural prediction
Alphafold3
Pymol
Optimal
The binding of bait protein to IL-2
Score verification
c
B0
B34
B51
G9
G16
G26
G32
G35
G42
G57
G63
G71
G88
G90
d
B0
B34
B51
G9
G16
G35
G42
G57
G71

Fig.1 | *De novo* design and selection of the IL-2 mimics. a, Structure of IL-2 (cartoon representation) in complex with the IL-2Rαβγ (surface representation) (PDB ID: 2B5I) with their binding interfaces. **b,** Schematic illustration of the design and score verification process for RFdiffusion conjugates. Amino acid residue "noise" is processed via the RFdiffusion model to generate synthetic proteins with diverse geometries for β and γ bait protein respectively. As for the binding of bait protein to IL-2, molecular docking (via HDOCK) and structural prediction (via AF3) are conducted, followed by scoring to determine the optimal result, which is then visualized through PyMOL. **c,** The front view of the binding sites between screened mimics with IL-2Rβ and γ separately. **d,** Binding interfaces between the trimmed sequences and the IL-2Rβ and γ respectively, with the box zooming in to show the amino acids at the binding site (stick representation).

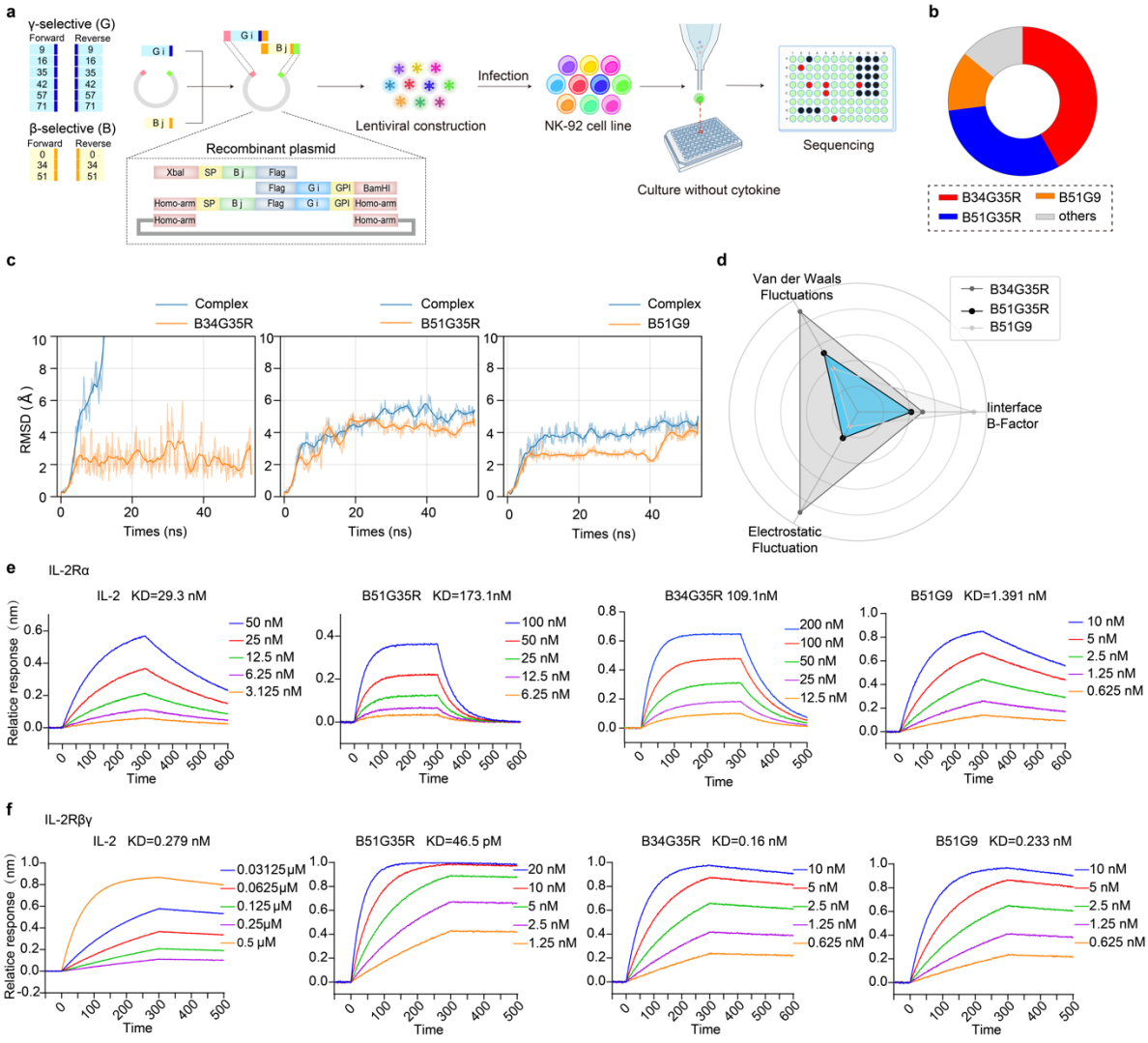

Fig.2 | Screening and Affinity Detection. **a,** Construction and screening of IL-2 mimics library. Twelve IL-2Rβ binding mimics six IL-2Rγ mimics form 36 combinations. Sequencing was employed to screen the best complexes. **b**, Pie chart shows the significant enrichment of B34G35R, B51G9 and B51G35R where area corresponds to enrichment level. **c,** RMSD profiles of the complex (B34G35R, B51G35R, B51G9) fluctuate around 4 Å as a function of simulation time for 50 ns). The blue row represents the IL-2 as control while orange row indicates our IL-2 mimics. **d,** MD simulations based on down-selection using criteria such as fluctuations in electrostatic and van der Waals interactions combined with an interface-residue-B-factor analysis as estimators for conformational flexibility in the binding interface identify B51G9 (cyan) as the most promising IL-2 mimics. For each mimic, 1×50 ns were calculated. **e-f**, BLI characterization of the binding of designed proteins to the IL-

2Rα (e) and IL-2Rβγ (f) respectively. Twofold serial dilutions were tested for each binder and all concentration are labelled. The IL-2 mimics were loaded onto streptavidin biosensors, and incubated with designed binders in solution to measure association and dissociation.

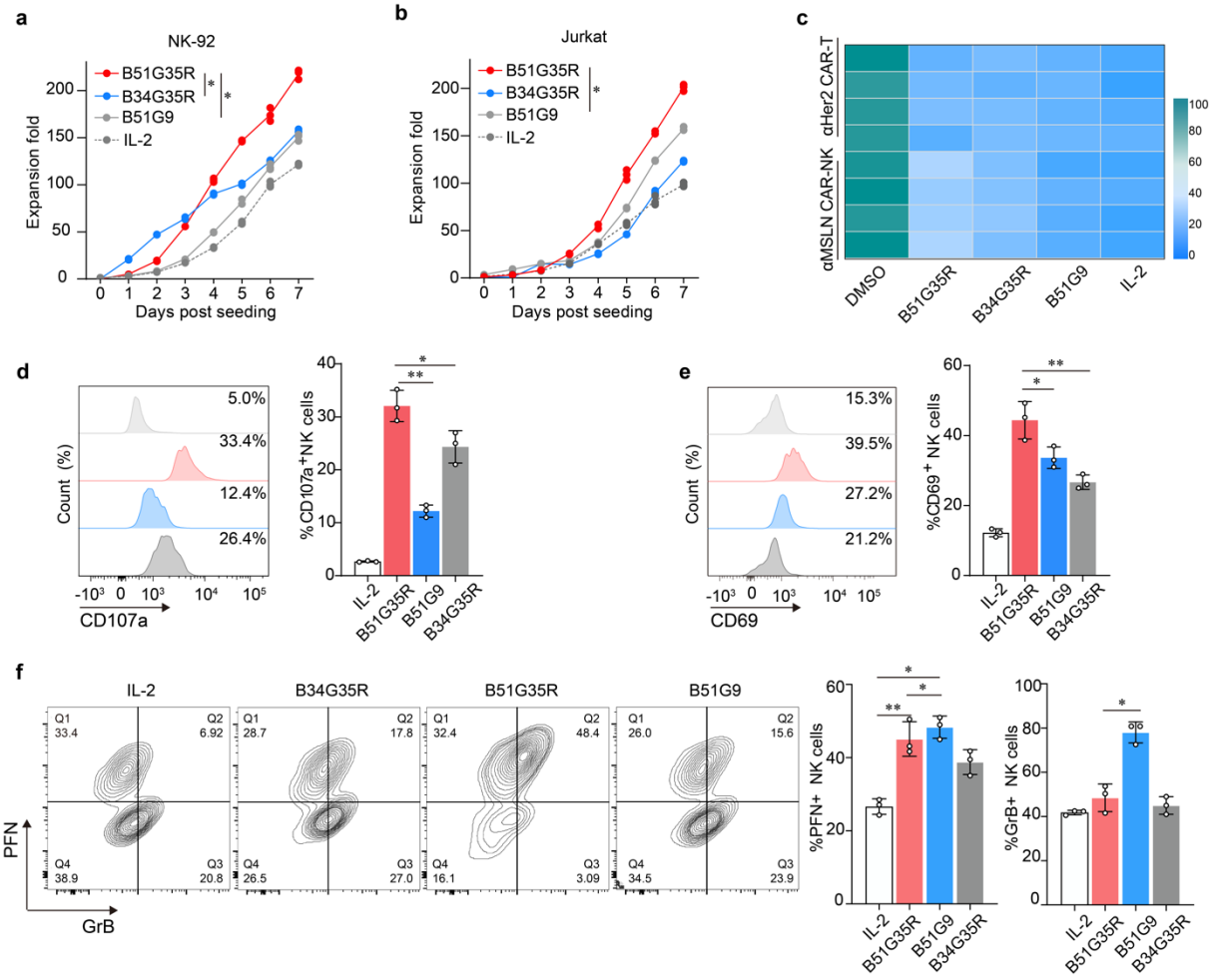

Fig.3 | Proliferation and *in vitro* antitumor effect of the screened sequences. a-b, Proliferation activity of NK-92 cells and YT cells in response to B34G51, B34G35, B51G9 and IL-2 stimulation. Data are presented as mean ± SD of three independent biological replicates (*$P < 0.05$). **c,** The cytotoxic capabilities of αMSLN CAR-NK and αHER2 CAR-T expressing IL-2 mimics. DMSO was utilized as positive control. **d-e,** CD107a and CD69 expression were analyzed in effector cells which equipped with IL-2 and its mimics. Data are representative of three independent experiments (**$P <$ 0.01, *$P < 0.05$). **f,** The PFN and GrB expression levels were assessed by flow cytometry. Data are representative of at least three independent experiments (**$P <$ 0.01, *$P < 0.05$).

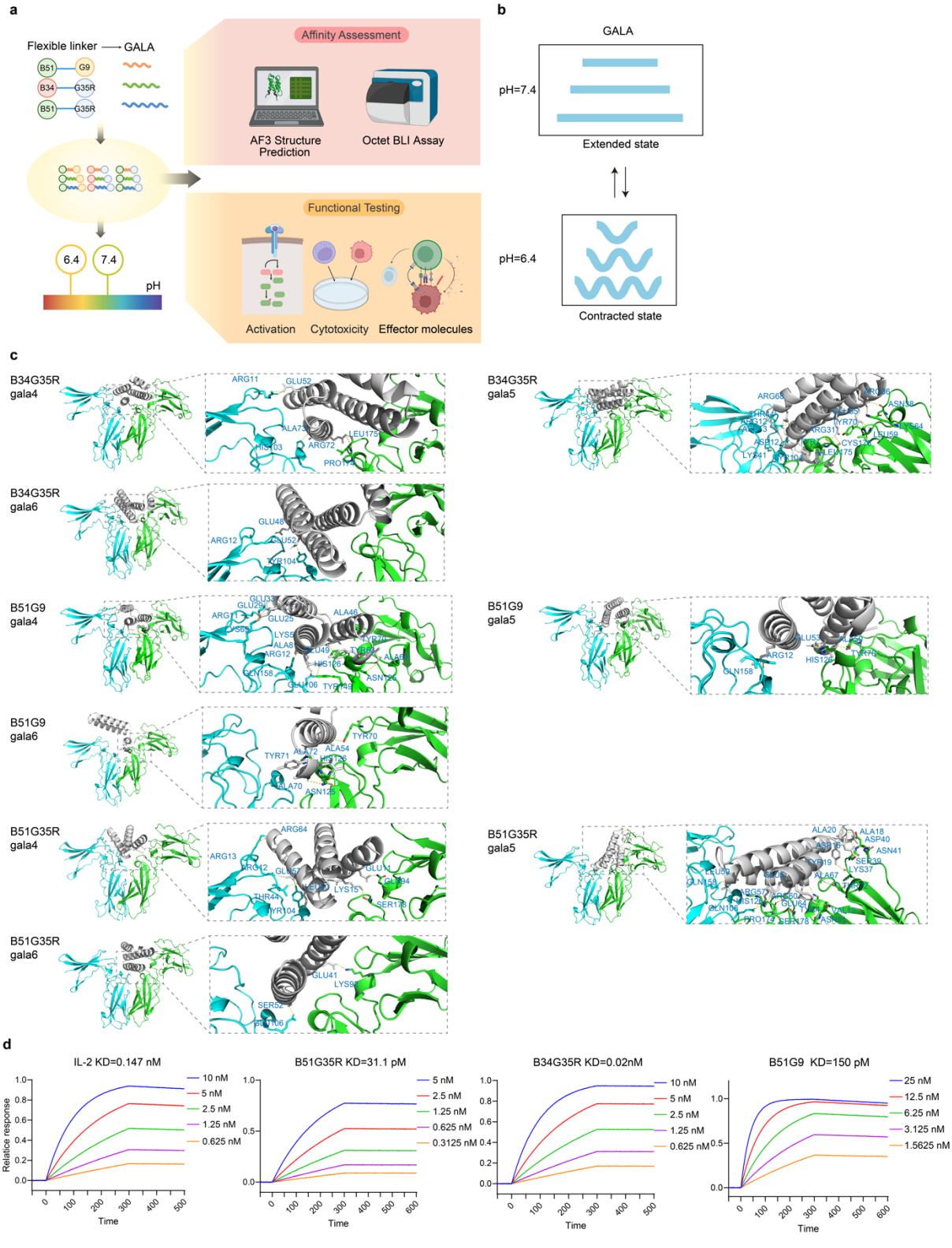

Fig.4 | GALA replacement and detection of binding affinity under acidic condition.

a, Schematic overview of the replacement of GALA, affinity assessment through AF3 structure prediction and BLI assay, and functional testing including activation, cytotoxicity and effector molecules of the designed mimics with where the flexible

GGGGS peptide was substituted with GALA4, GALA 5, GALA 6 (4, 5, and 6 represent the number of EALA repeat units in the GALA peptide). **b,** General depiction of the conformational transition of GALA between extended state at pH=7.4 and contracted state at pH=6.4. **c,** The front view of the binding sites between B34G35R-G, B51G35R-G, and B51G9-G with IL-2Rβγ, with the box zooming in to show the amino acids at the binding site (stick representation). **d,** BLI characterization of the binding of B34G35R-G, B51G35R-G, and B51G9-G to IL-2Rβγ.

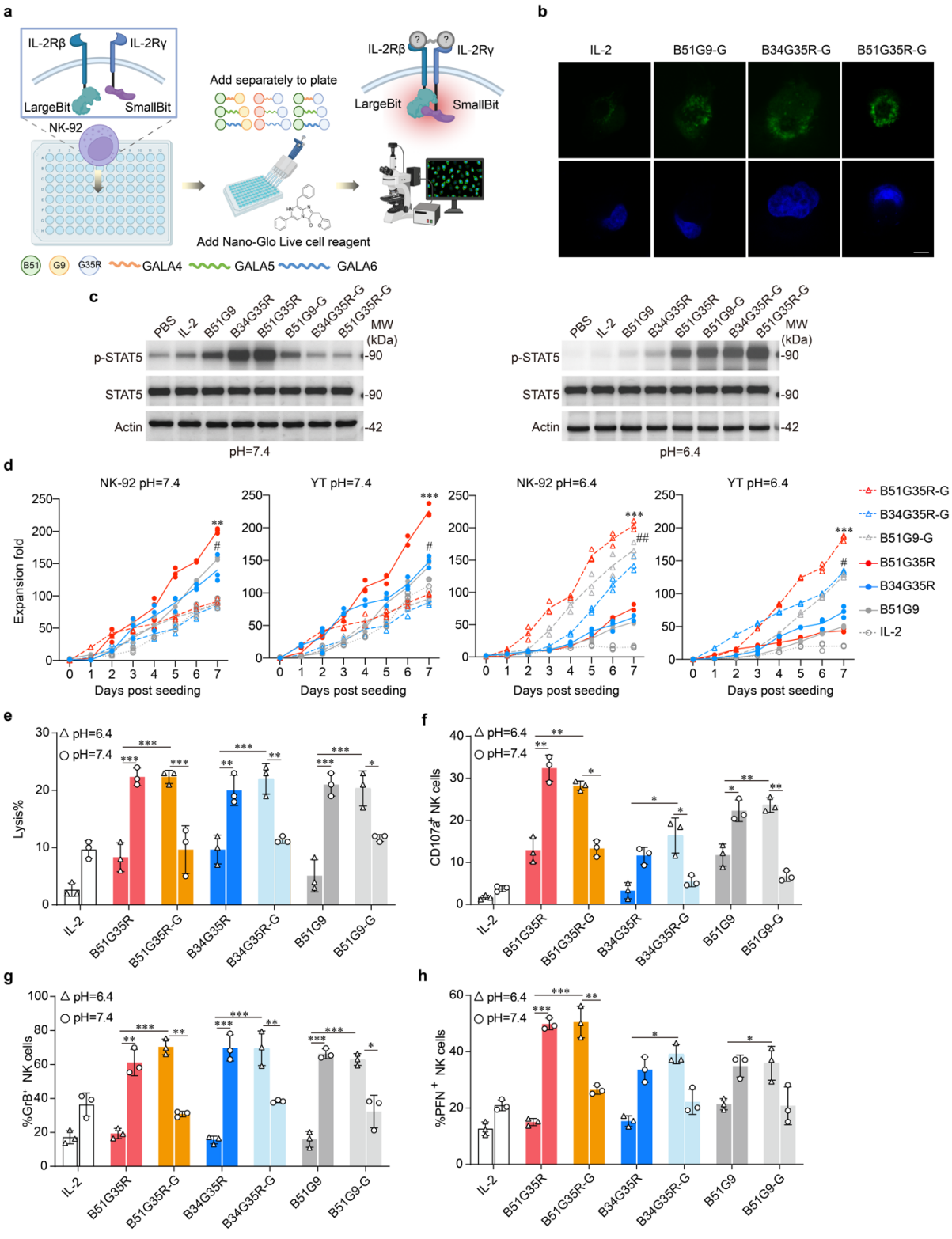

Fig.5 | Effects of B34G35R-G, B51G35R-G, and B51G9-G on NK cell proliferation and *in vitro* anti-tumor activity. a, Illustration of the NanoBiT protein complementation assay. The oligomerization induced by fusing LargeBit and SmallBit to IL-2Rβ and IL-2Rγ was verified through immunofluorescence. **b,** Fluorescence

microscopy was utilized to capture images of the NK cells. The green fluorescence indicated the NK-92 cells and the blue fluorescence indicated DAPI, scale bar = 20 μM. **c,** Expansion fold of NK-92 cells and YT cells at pH=7.4 and pH=6.4 over days post seeding for different constructs (B51G35R-G, B34G35R-G, B51G9-G, B51G35R, B34G35R, B51G9, IL-2). Data are presented as mean ± SD of three independent biological replicates. **d,** LDH tests for Lysis detection of NK cells expressing IL-2, B51G35R, B51G35R-G, B34G35R, B34G35R-G, B51G9, B51G9-G separately at both pH=6.4 and pH=7.4. Data are representative of at least three independent experiments. **e-g,** Flow cytometry for CD107a, PFN, GrB detection of NK cells with IL-2 and IL-2 mimics separately at both pH=6.4 and pH=7.4. Data are representative of at least three independent experiments (*$P < 0.05$, **$P < 0.01$, ***$P < 0.001$,).

Reference

1. E. Liu *et al.*, Use of CAR-Transduced Natural Killer Cells in CD19-Positive Lymphoid Tumors. *N Engl J Med* **382**, 545-553 (2020).
2. Y. Liu *et al.*, An Injectable Puerarin Depot Can Potentiate Chimeric Antigen Receptor Natural Killer Cell Immunotherapy Against Targeted Solid Tumors by Reversing Tumor Immunosuppression. *Small* **20**, e2307521 (2024).
3. V. Narayan *et al.*, PSMA-targeting TGFβ-insensitive armored CAR T cells in metastatic castration-resistant prostate cancer: a phase 1 trial. *Nat Med* **28**, 724-734 (2022).
4. K. Beider *et al.*, Involvement of CXCR4 and IL-2 in the homing and retention of human NK and NK T cells to the bone marrow and spleen of NOD/SCID mice. *Blood* **102**, 1951-1958 (2003).
5. K. Pance *et al.*, Modular cytokine receptor-targeting chimeras for targeted degradation of cell surface and extracellular proteins. *Nat Biotechnol* **41**, 273-281 (2023).
6. X. Hu, J. Li, M. Fu, X. Zhao, W. Wang, The JAK/STAT signaling pathway: from bench to clinic. *Signal Transduct Target Ther* **6**, 402 (2021).
7. J. L. Ptacin *et al.*, An engineered IL-2 reprogrammed for anti-tumor therapy using a semi-synthetic organism. *Nat Commun* **12**, 4785 (2021).
8. R. Hernandez, J. Põder, K. M. LaPorte, T. R. Malek, Engineering IL-2 for immunotherapy of autoimmunity and cancer. *Nat Rev Immunol* **22**, 614-628 (2022).
9. R. Baluna, E. S. Vitetta, Vascular leak syndrome: a side effect of immunotherapy. *Immunopharmacology* **37**, 117-132 (1997).

10. J. Shu, When cellular reprogramming meets AI: towards *de novo* cell design. *Nat Rev Genet* **26**, 585 (2025).
11. K. H. Johansen *et al.*, *De novo*-designed pMHC binders facilitate T cell-mediated cytotoxicity toward cancer cells. *Science* **389**, 380-385 (2025).
12. G. Rojas *et al.*, Molecular reshaping of phage-displayed Interleukin-2 at beta chain receptor interface to obtain potent super-agonists with improved developability profiles. *Commun Biol* **6**, 828 (2023).
13. S. Vázquez Torres *et al.*, *De novo* design of high-affinity binders of bioactive helical peptides. *Nature* **626**, 435-442 (2024).
14. X. Wang, M. Rickert, K. C. Garcia, Structure of the quaternary complex of interleukin-2 with its alpha, beta, and gammac receptors. *Science* **310**, 1159-1163 (2005).
15. M. Akdis *et al.*, Interleukins, from 1 to 37, and interferon-γ: receptors, functions, and roles in diseases. *J Allergy Clin Immunol* **127**, 701-721.e701-770 (2011).
16. J. D. Fontenot, J. P. Rasmussen, M. A. Gavin, A. Y. Rudensky, A function for interleukin 2 in Foxp3-expressing regulatory T cells. *Nat Immunol* **6**, 1142-1151 (2005).
17. A. M. Levin *et al.*, Exploiting a natural conformational switch to engineer an interleukin-2 'superkine'. *Nature* **484**, 529-533 (2012).
18. C. A. Sarkar *et al.*, Rational cytokine design for increased lifetime and enhanced potency using pH-activated "histidine switching". *Nat Biotechnol* **20**, 908-913 (2002).
19. J. B. Spangler, I. Moraga, J. L. Mendoza, K. C. Garcia, Insights into cytokine-receptor interactions from cytokine engineering. *Annu Rev Immunol* **33**, 139-167 (2015).
20. K. G. Anderson, I. M. Stromnes, P. D. Greenberg, Obstacles Posed by the Tumor Microenvironment to T cell Activity: A Case for Synergistic Therapies. *Cancer Cell* **31**, 311-325 (2017).
21. O. Trédan, C. M. Galmarini, K. Patel, I. F. Tannock, Drug resistance and the solid tumor microenvironment. *J Natl Cancer Inst* **99**, 1441-1454 (2007).
22. M. Yang, J. Li, P. Gu, X. Fan, The application of nanoparticles in cancer immunotherapy: Targeting tumor microenvironment. *Bioact Mater* **6**, 1973-1987 (2021).
23. P. F. Gao, J. J. Cui, J. M. Li, B. F. Zhang, Dextran-based prodrug-nanoassemblies responsively releasing pidotimod and camptothecin for anti-breast cancer. *Drug Dev Ind Pharm*, 1-10 (2025).
24. Y. Y. Gong *et al.*, Na(+)/H(+)-exchanger 1 enhances antitumor activity of engineered NK-92 natural killer cells. *Cancer Res Commun* **2**, 842-856 (2022).
25. T. Shi *et al.*, Acidity-targeting transition-aided universal chimeric antigen receptor T-cell (ATT-CAR-T) therapy for the treatment of solid tumors. *Biomaterials* **309**, 122607 (2024).
26. T. Sulea *et al.*, Structure-based engineering of pH-dependent antibody binding for selective targeting of solid-tumor microenvironment. *MAbs* **12**, 1682866 (2020).

27. T. Fang *et al.*, Bioresponsive and immunotherapeutic nanomaterials to remodel tumor microenvironment for enhanced immune checkpoint blockade. *Bioact Mater* **32**, 530-542 (2024).
28. B. Wang *et al.*, IL-21 Loading CaMnCO(3) Vitality Backpacks Boost CAR-T Cell Synergistic Immunotherapy. *Small* **21**, e2501645 (2025).